Linear optical properties of gold nanoshells

Richard D. Averitt,* Sarah L. Westcott, and Naomi J. Halas

Department of Electrical and Computer Engineering and the Center for Nanoscale Science and Technology, Rice University, Houston, Texas 77005

Received March 22, 1999; revised manuscript received June 29, 1999

A metal nanoshell consists of a nanometer-scale dielectric core surrounded by a thin metallic shell. The plasmon resonance of metal nanoshells displays a geometric tunability controlled by the ratio of the core radius to the total radius. For gold-coated Au_2S this ratio varies from 0.6 to 0.9, yielding a plasmon resonance tunable from 600 to greater than 1000 nm. Mie scattering theory for the nanoshell geometry quantitatively accounts for the observed plasmon resonance shifts and linewidths. In addition, the plasmon linewidth is shown to be dominated by electron surface scattering. © 1999 Optical Society of America [S0740-3224(99)02910-0]

OCIS codes: 260.3910, 290.4020, 240.6680, 290.3700, 260.5740.

1. INTRODUCTION

Solid metal nanoparticles display a wide range of interesting and potentially useful properties, optical and otherwise, that motivate the current research activity related to these systems.[1] From a fundamental point of view, metal nanoparticles bridge the gap between the atomic level and the bulk, exhibiting mesoscopic properties unique to this size regime. The most ubiquitous of these is the optical plasmon resonance associated with the collective oscillation of the conduction electrons confined in the nanoparticle. For example, solid gold nanoparticles have a strong optical absorption at 520 nm, and silver nanoparticles have a resonance at 390 nm. This plasmon resonance is sensitive to the local chemical environment at the nanoparticle interface, leading to the possibility of sensitive optically based chemical detectors.[2,3,4] There is local optical field enhancement associated with the plasmon resonance, which is important in surface-enhanced Raman scattering and surface second-harmonic generation.[5,6] Metal nanoparticles also display a large and fast third-order optical nonlinearity, making them candidates in future all-optical switching devices.[7]

Recently there has been tremendous progress in the fabrication, functionalization, and characterization of solid metal nanoparticles.[8] New fabrication methods reduce the nanoparticle size distribution, which improves the optical properties of metal nanoparticles by reducing inhomogeneous broadening. Equally important, these new fabrication techniques facilitate the incorporation of metal nanoparticles into functional devices, with a particular emphasis on the fabrication of metal nanoparticle arrays.[9,10] In metal nanoparticle arrays there can be classical dipole–dipole coupling or quantum mechanical (i.e., tunneling) coupling between the individual nanoparticles, depending on the interparticle distance.[11,12] This leads to interesting phenomena such as the observation of a distance-dependent tunable metal insulator transition in silver nanoparticle arrays.[11] The ability to control the interactions between nanoparticles precisely is certain to lead to new applications.

Another important direction of research into the properties of individual metal nanoparticles involves controlled variation of the nanoparticle geometry. This can yield new and tunable optical properties that solid metal nanoparticles do not possess.[13] Metal nanoshells are a prime example of this strategy. The geometry of metal nanoshells is shown in Fig. 1. Metal nanoshells consist of a nanometer-scale dielectric core with radius r_1 surrounded by a thin metal shell of thickness $r_2 - r_1$. Metal nanoshells exhibit a geometric tunability, characterized by the ratio of the core radius to the total radius (r_1/r_2), that effectively extends the optical properties of metal nanoparticles from the visible into the infrared. A theoretical description of the optical properties of metal nanoshells, based on Mie scattering theory, has existed for some time.[14,15] However, it is only in the past few years that metal nanoshells have been experimentally realized.[16,17,18]

In this paper we present the results of our optical studies of gold-coated Au_2S nanoshells. The plasmon resonance of gold-coated Au_2S nanoshells displays the expected geometric tunability described above. For gold-coated Au_2S nanoshells the ratio of r_1/r_2 can be varied from 0.6 to 0.9, yielding a plasmon resonance tunable from 600 nm to greater than 1000 nm. In addition, the plasmon linewidth is shown to be dominated by electron surface scattering with a smaller contribution resulting from a population size distribution of nanoshells. We also discuss the effect of electron surface scattering on the reduction of the local-field enhancement associated with metal nanoshells.

2. EXPERIMENT

The growth of gold nanoshells is initiated when aqueous solutions of $HAuCl_4$ and Na_2S are mixed. American Chemical Society reagent-grade $HAuCl_4$ and Na_2S were obtained from Sigma. All chemicals were used as purchased. Deionized Millipore TotalQ water was used for the reactions. All glassware was cleaned with chromic acid and rinsed with deionized water. The typical reaction was started when 1 mM Na_2S was mixed in 2 mM $HAuCl_4$ with volume ratios ranging from 1.2:1 to 1.6:1.

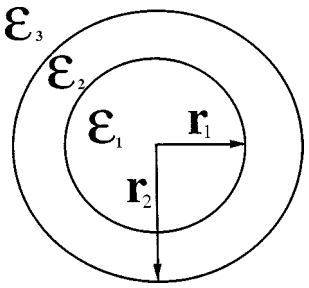

Fig. 1. Nanoshell geometry: ϵ_i ($i = 1, 2, 3$) are the dielectric functions for the core, shell, and embedding regions, respectively. r_1 is the core radius, and r_2 is the total particle radius.

Previously, we proposed the following reaction for the initial reduction process[17]:

$$2AuCl_4^- + 3HS^- \rightleftharpoons 2Au + 3S + 3H^+ + 8Cl^-. \quad (1)$$

Au and S were then available for subsequent nucleation and growth. It was important to use Na_2S solutions 1–2 days after they were made. When fresh Na_2S solutions were used, the reaction would not proceed. This might have been because fresh solutions have low HS^- activity. If Na_2S solutions were used that were older than approximately 2 days, the reaction would still proceed but comparatively not as well as with the use of the 1–2-day-old Na_2S solutions. This could have been due in part to complicated aqueous sulfur chemistry involving the formation of polysulfides.[19] No such aging problems were observed for the $HAuCl_4$ solutions.

Both solid gold nanoparticles and gold-coated Au_2S nanoparticles formed when the Na_2S and the $HAuCl_4$ were mixed. The reaction was monitored by the UV-visible absorption spectrum of the solution. Figure 2(a) shows a series of UV-visible spectra taken with a Hitachi U2001 spectrophotometer as a typical reaction proceeded to completion. The absorption feature at 520 nm is due to the plasmon resonance of the solid gold nanoparticles, whereas the longer wavelength feature is due to the gold–gold sulfide nanoshells.[16,17] Figure 2(b) shows the nanoshell resonance wavelength and the linewidth as a function of time. The resonance initially appeared at ~700 nm and then shifted to ~920 nm; after 22 min a pronounced blueshift ensued, leaving the resonance at 680 nm at the end of the reaction. As the reaction progressed, the FWHM of the gold nanoshell resonance narrowed from ~0.70 eV at 9 min to ~0.42 eV at 80 min.

For the reaction shown in Fig. 2 the plasmon resonance was at 680 nm at the end of the reaction. It was possible to control the final resonance wavelength by variation of the starting reactant concentrations. A slight decrease in the ratio of sulfur to gold (e.g., 1.4 decreased to 1.3) resulted in a plasmon resonance that was shifted to longer wavelengths, whereas an increase in the ratio yielded a more strongly blueshifted resonance at the end of the reaction. With this method we have been able to control the placement of the plasmon resonance over a range extending from 650 to greater than 1000 nm. Another approach was to stop the nanoparticle growth by the addition of a ligand to the solution that terminated the nanoshell surface. For example, we have used $P(C_6H_4SO_3Na)_3$ to quench the reaction and stop the corresponding plasmon resonance shift. This ligand has been found to impart exceptional stability to solid gold colloid.[20] The phosphorus atom covalently bonds to the gold surface, whereas the charged SO_3^- groups give the colloid a net negative charge, preventing permanent aggregation that is due to dispersional van der Waals forces. If the ligand was added too early during the reaction (i.e., during the initial shift of the plasmon resonance to longer wavelengths), the colloids flocculated.

Transmission electron microscopy was performed on gold nanoshell samples with a JEOL JEM-2010 transmission electron microscope (TEM) operating at 100 or 200 kV. Samples were prepared by placement of a drop of the nanoshell colloidal solution on a carbon-coated copper grid that was placed on filter paper to remove the excess liquid. Figure 3(a) shows a TEM picture of a gold nanoshell sample. The larger particles are the gold-coated Au_2S nanoparticles, and the smaller particles are solid gold. Repeated attempts to directly image the shell were not successful. This could be in part due to drift problems associated with the TEM and contrast difficul-

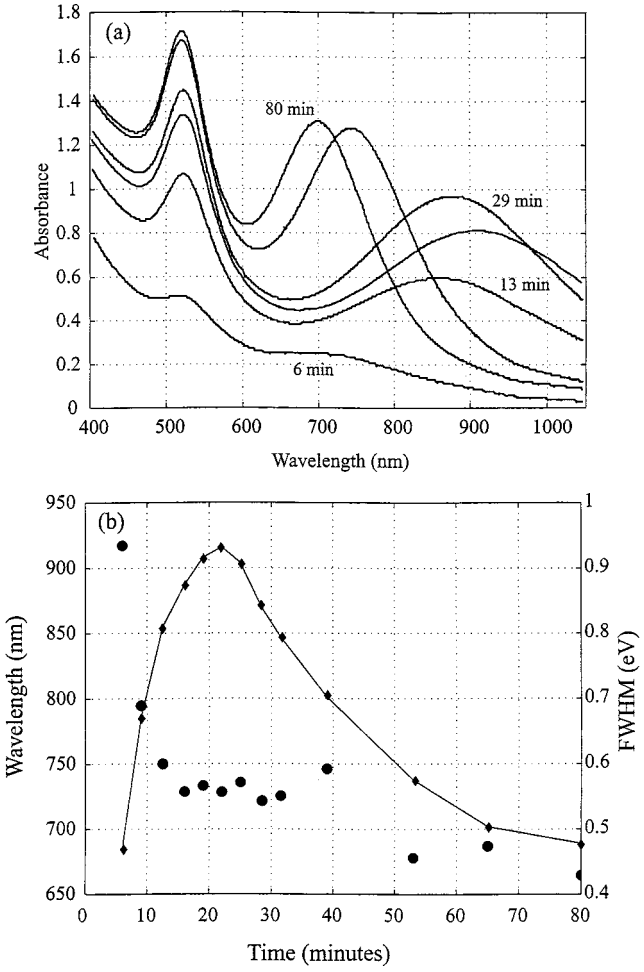

Fig. 2. (a) UV-visible absorption spectra of gold-coated Au_2S nanoshells during the course of the reaction, showing the plasmon resonance shifts and the linewidth changes. (b) The metal nanoshell plasmon resonance wavelength (diamonds, left axis) and linewidth (circles, right axis) as a function of time. The curve is to guide the eye. Fig. 2(a) was presented previously in Ref. 17.

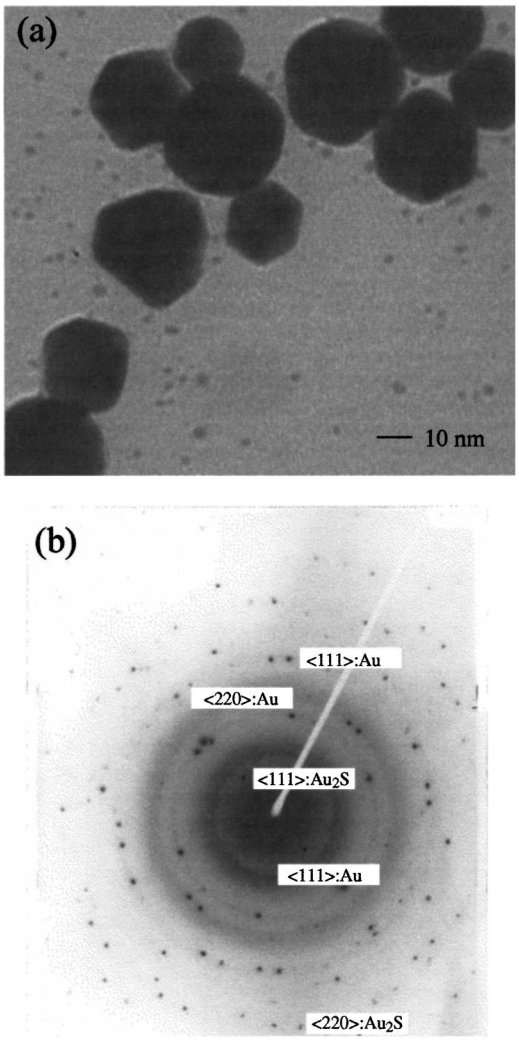

Fig. 3. (a) Transmission electron micrograph of the larger gold-coated Au_2S nanoshells and accompanying smaller solid gold nanoparticles. (b) Electron diffraction pattern of a nanoshell sample. Sharp Bragg peaks correspond to various plane spacings of gold and Au_2S, as labeled.

ties in imaging a thin shell on a large core. It should be noted that Zhou *et al.* did obtain a TEM image of the shell.[16]

Figure 3(b) is a TEM electron diffraction micrograph of a nanoshell sample. There are three rings of spots that correspond to plane spacings of gold along the directions indicated in the figure. There are also two rings that correspond to the plane spacing of Au_2S along the $\langle 111 \rangle$ and $\langle 220 \rangle$ directions. The sharp spots indicate that the material is crystalline, although the presence of the dim rings indicates a degree of polycrystallinity. This shows that the nanoshell samples are comprised of gold and Au_2S. However, the diffraction pattern is not direct proof that the large particles are gold-coated because there may also have been diffraction from neighboring small gold nanoparticles in the sample.

The size distribution of the solid gold nanoparticles and the gold-coated Au_2S nanoparticles was determined from transmission electron micrographs. Each TEM image contained about a hundred particles, from which a histogram was obtained with Image Tool to measure the diameter of each particle.[21] The solid gold nanoparticles had an average diameter of ~3 nm and the gold-coated Au_2S nanoparticles had an average diameter of 40 nm at the end of the reaction. The standard deviation for size distributions of both the solid gold nanoparticles and the gold-coated Au_2S nanoparticles ranged from ±15 to ±20 percent in different samples.

3. LINEAR OPTICAL PROPERTIES OF NANOSHELLS

A. Introduction: Mie Scattering Theory

The observed plasmon resonance shift and linewidth narrowing shown in Fig. 2(b) can be understood with Mie scattering theory.[22] Mie theory is the solution of Maxwell's equations in spherical coordinates with boundary conditions appropriate for a sphere. In the modern approach to this problem the solutions to Maxwell's equations for the fields are expressed in a series expansion of vector eigenfunctions that form a complete set.[23–27] Mie theory beautifully explains the ruby–red color of colloidal gold: Colloidal gold has a plasmon resonance at 520 nm that is due to the collective excitation of electrons that are coupled to the transverse electromagnetic field. The electrons oscillate with respect to the positive ionic cores, and it is the surface polarization that provides a restoring force.

Mie theory requires that the dielectric function of the particle and the embedding medium be specified. Thus Mie theory is phenomenological in character in that it provides no physical insight into material properties other than what is specified by the input dielectric function. There are two distinct size regimes to consider in the determination of the electromagnetic properties of metallic nanoparticles.[1] In the extrinsic size regime the optical properties can be fully described by specification of the nanoparticle radius and by use of the bulk frequency-dependent dielectric constant $\epsilon(\omega)$. For solid gold nanoparticles this so-called extrinsic regime occurs for diameters greater than ~50 nm. In this regime, size-dependent effects are purely electromagnetic. For example, as a function of increasing size, contributions from higher-order multipoles and phase retardation effects become important. The relative contribution of scattering to the total cross section increases, and the plasmon resonance broadens. Conversely, in the intrinsic size regime ($2r < 50$ nm), dipole plasmon absorption is by far the dominant contribution to the extinction cross section. Thus size-dependent effects must be accounted for by employment of a size-dependent dielectric function $\epsilon(\omega, r)$, where r is the nanoparticle radius. This is an important regime for two reasons. First, information about changes in the electronic and the optical properties are reflected in the respective changes in $\epsilon(\omega, r)$. Second, $r \ll \lambda$ (wavelength), and the quasi-static approach can be employed in the calculations. In quasi-static calculations the spatial variation of the electromagnetic field is neglected while the temporal dependence is preserved, considerably simplifying the calculations.

Conceptually, the extension of Mie theory to a metallic shell is quite simple: One must simply specify the boundary conditions at one additional interface. The

shell-core system depicted in Fig. 1 has been studied with Mie scattering theory, and expressions for the polarizability and the extinction cross section of shell-core particles have been derived.[1,14,26] Rather than present the details of Mie theory for a shell-core geometry, Subsection 3.B derives the absorption and the extinction cross sections for nanoshells in the quasi-static limit. Quasi-static calculations will be compared with Mie theory calculations to show the validity of using the quasi-static results. Furthermore, the quasi-static equations are useful in the calculation of nonlinear optical effects in nanoshells.[15]

Two simplifying assumptions are used in our analysis. As shown in Fig. 3(a), the nanoshells are not perfectly spherical, but it considerably simplifies the analysis to treat them as such. Also, interactions between nanoparticles (e.g., dipole–dipole) will not be considered, since the nanoshell concentration is in the nanomolar range.

B. Quasi-Static Theory of Nanoshells

We first present a brief derivation of the electromagnetic properties of a metallic shell. The expressions for the electric fields and the polarizability were derived by others,[14,15,28] but here we present explicit formulas for the scattering and the absorption cross sections in addition to the geometric tunability of the resonant properties of metal nanoshells. It is assumed that the particle diameter is much smaller than the wavelength of the incident field. The incident field is time dependent, but it does not vary spatially over the diameter of the metal shell. In this case, the electrostatic solution can be obtained by solution of Laplace's equation for the potential.

The geometry is as shown in Fig. 1. Region 1 is the core and is characterized by a radius r_1 and dielectric function ϵ_1. The shell has a thickness $r_2 - r_1$ and a dielectric function ϵ_2. The embedding medium has a dielectric function ϵ_3. It is important to note that, at this point, none of the dielectric functions ϵ_i $(i = 1, 2, 3)$ have been specified. Each can have real and imaginary frequency-dependent components. The geometry becomes that of a metal nanoshell when ϵ_2 is specified as the dielectric function of a metal and the core is, nominally, a dielectric material.

The general solution for the potential in each region is given by

$$\Phi_i(r, \theta) = [A_i r + (B_i/r^2)]\cos\theta, \tag{2}$$

where A_i and B_i are the constants multiplying the monopole and the dipole terms, respectively.

The boundary conditions must be specified so that the potential in the core, shell, and embedding medium can be determined. First, there must be continuity of the tangential component of the electric field:

$$\left.\frac{\partial\Phi_i}{\partial\theta}\right|_{r=r_i} = \left.\frac{\partial\Phi_{i+1}}{\partial\theta}\right|_{r=r_i}. \tag{3}$$

Second, there must be continuity of the normal component of the displacement field:

$$\epsilon_i\left.\frac{\partial\Phi_i}{\partial r}\right|_{r=r_i} = \epsilon_{i+1}\left.\frac{\partial\Phi_{i+1}}{\partial r}\right|_{r=r_i}. \tag{4}$$

In region 1, $B_1 = 0$; in region 3, far from the shell, we must recover the potential $\Phi_3 = -E_o r\cos\theta$, thus giving $A_3 = -E_o$. With A_3 and B_1 determined, application of the boundary conditions to Eq. (2) results in a set of four equations and four unknowns that can be solved to obtain A_1, A_2, B_2, and B_3. Then the electric field in each region can be obtained with $E_i = -\nabla\Phi_i(r, \theta)$. This results in the following equations for the fields:

$$\mathbf{E}_1 = \frac{9\epsilon_2\epsilon_3}{\epsilon_2\epsilon_a + 2\epsilon_3\epsilon_b}E_o(\cos\theta\hat{r} - \sin\theta\hat{\theta}), \tag{5}$$

$$\mathbf{E}_2 = \frac{3\epsilon_3}{\epsilon_2\epsilon_a + 2\epsilon_3\epsilon_b}\{[(\epsilon_1 + 2\epsilon_2) + 2(\epsilon_1 - \epsilon_2) \times (r_1/r)^3]E_o\cos\theta\hat{r} - [(\epsilon_1 + 2\epsilon_2) - (\epsilon_1 - \epsilon_2)(r_1/r)^3]E_o\sin\theta\hat{\theta}\}, \tag{6}$$

$$\mathbf{E}_3 = \left(2\frac{\epsilon_2\epsilon_a - \epsilon_3\epsilon_b}{\epsilon_2\epsilon_a + 2\epsilon_3\epsilon_b}\frac{r_2^3}{r^3} + 1\right)E_o\cos\theta\hat{r} + \left(\frac{\epsilon_2\epsilon_a - \epsilon_3\epsilon_b}{\epsilon_2\epsilon_a + 2\epsilon_3\epsilon_b}\frac{r_2^3}{r^3} - 1\right)E_o\sin\theta\hat{\theta}, \tag{7}$$

where

$$\epsilon_a = \epsilon_1(3 - 2P) + 2\epsilon_2 P, \tag{8}$$

$$\epsilon_b = \epsilon_1 P + \epsilon_2(3 - P), \tag{9}$$

$$P = 1 - (r_1/r_2)^3. \tag{10}$$

P is the ratio of the shell volume to the total particle volume. The notation for the fields follows Neeves and Birnboim.[15]

The induced field in the region outside the shell is the same as a dipole with an effective dipole moment given by $\mathbf{p} = \epsilon_3\alpha\mathbf{E}_{\text{ind}}$. The polarizability is then given as follows:

$$\alpha = 4\pi\epsilon_o r_2^3\left[\frac{\epsilon_2\epsilon_a - \epsilon_3\epsilon_b}{\epsilon_2\epsilon_a + 2\epsilon_3\epsilon_b}\right], \tag{11}$$

where $\epsilon_o = 8.85 \times 10^{-12}$ F/m is the permittivity of free space.

Finally, we can obtain the absorption and the scattering cross sections from the polarizability by using scattering theory.[29] For the scattering cross section we obtain

$$\sigma_{\text{sca}} = \frac{1}{6\pi\epsilon_o^2}k^4|\alpha|^2, = \frac{128\pi^5}{3\lambda^4}\epsilon_3^2 r_2^6\left|\frac{\epsilon_2\epsilon_a - \epsilon_3\epsilon_b}{\epsilon_2\epsilon_a + 2\epsilon_3\epsilon_b}\right|^2, \tag{12}$$

where the approximation for the index of refraction $\tilde{n} = \sqrt{\epsilon_3}$ has been made. This is valid in the limit of low concentration of nanoshells. Similarly, the absorption cross section is given as follows:

$$\sigma_{\text{abs}} = \frac{k}{\epsilon_o}\text{Im}(\alpha), = \frac{8\pi^2\sqrt{\epsilon_3}}{\lambda}r_2^3\,\text{Im}\left(\frac{\epsilon_2\epsilon_a - \epsilon_3\epsilon_b}{\epsilon_2\epsilon_a + 2\epsilon_3\epsilon_b}\right). \tag{13}$$

With Eqs. (12) and (13) the calculations of the extinction cross section for gold nanoshells are shown in Fig. 4(a). The results of these calculations (shown as circles) are for a constant shell thickness of 2 nm and $r_2 = 4$, 10, and 17 nm. The core dielectric constant was determined by use of an estimate of the calculated bandgap of Au_2S (Ref. 30) (2.6 eV) and the empirical expression $\epsilon^2 E_g = 77$, where ϵ is the dielectric constant and E_g is the bandgap.[31] In our analysis we have treated the Au_2S core as a nonabsorbing dielectric. No features in the absorption spectrum are attributable to the Au_2S core. For the surrounding aqueous medium we use the value $\epsilon_3 = 1.78$. For the shell permittivity $\epsilon_2(\omega)$ we use the experimentally measured bulk values for gold.[32] Figure 4(a) reveals the most important characteristic of metal nanoshells: The plasmon absorption resonance wavelength depends on the ratio of the core radius r_1 to the total radius r_2. For a given shell thickness a larger r_2 will yield a plasmon resonance that is shifted to longer wavelengths relative to a smaller r_2.

The solid curves in Fig. 4(a) are the results of Mie scattering calculations with the same parameters as the quasi-static calculations. For these calculations ten terms in the multipole expansion were used.[1,14,26] The resulting good agreement justifies the use of quasi-static calculations for gold nanoshells with diameters less than ~50 nm.

From Eq. (11) we can see that the resonance condition for a nanoshell is obtained when the real portion of the denominator goes to zero, that is, when $\mathrm{Re}(\epsilon_2 \epsilon_a + 2\epsilon_3\epsilon_b) = 0$. If the core and the embedding medium are dielectrics [i.e., $\mathrm{Im}(\epsilon_i) = 0$, $i = 1, 3$], then the following expression for the resonance condition as a function of wavelength is obtained:

$$\frac{r_1}{r_2} = \left[1 + \frac{3}{2}\,\frac{\epsilon_2'(\lambda)(\epsilon_1 + 2\epsilon_3)}{[\epsilon_2'(\lambda)]^2 - \epsilon_2'(\lambda)(\epsilon_1 + \epsilon_3) + \{\epsilon_1\epsilon_3 - [\epsilon_2''(\lambda)]^2\}}\right]^{1/3}. \quad (14)$$

This expression gives the ratio of the core radius to the total radius needed to obtain a resonant condition at a particular wavelength. This simple expression embodies the geometrical tunability that metallic nanoshells possess. The solid curve in Fig. 4(b) shows a plot of Eq. (14) for gold-coated Au_2S nanoshells. It should be remembered that Eq. (14) is valid only in the limit $r_2 \ll \lambda$ and $(r_2 - r_1)$ greater than a few atomic layers. The circles are calculations based on Mie theory, again showing good agreement with the quasi-static calculations. The *x*'s are Mie theory calculations that include line-broadening mechanisms that are discussed in Subsection 3.C. This shows that line-broadening effects are independent of the plasmon resonance shifts.

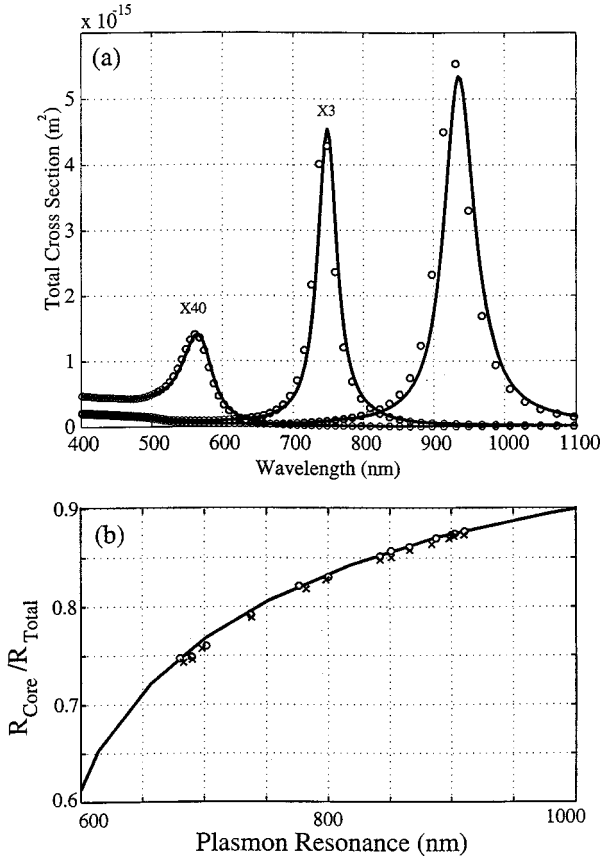

Fig. 4. (a) Total cross section versus wavelength for gold nanoshells with a 2-nm shell thickness. In going from shorter to longer wavelengths the total radius r_2 is 4, 10, and 17 nm, respectively. Circles, calculations in the quasi-static limit; solid curves, calculations based on generalized Mie scattering theory. (b) The ratio of the core radius to the total radius required to give a plasmon resonance at a specific wavelength.

C. Linewidth Considerations: Electron Surface Scattering

In Subsection 3.B the extinction cross section of gold nanoshells was calculated by use of the bulk dielectric function of gold. These calculations yield plasmon resonance linewidths (FWHM) of ~0.08 eV. As is shown in Fig. 2(b), this is much narrower than what was experimentally observed. Therefore line-broadening mechanisms must be considered if Mie theory is to describe the observed optical resonant properties of these nanoparticles adequately.

Various collisional processes are already embodied in the experimental bulk dielectric function for gold used in the analysis.[32] In bulk gold the conduction-electron mean free path at room temperature is ~42 nm.[33] Since these electrons travel at the Fermi velocity, which for gold is 1.4×10^8 cm/s, they have a collision frequency of $33.3 \times 10^{12}\ \mathrm{s}^{-1}$. This value includes electron–electron, electron–phonon, and electron–impurity interactions in the bulk. The experimentally measured dielectric function can be separated into contributions from Drude-like free electrons and interband transitions:

$$\varepsilon(\omega)_{\text{exp}} = \left(1 - \frac{{\omega_p}^2}{\omega^2 + i\omega\gamma_{\text{bulk}}}\right) + \varepsilon(\omega)_{\text{inter}}, \quad (15)$$

where the first term is the Drude free electron term, ω_p is the bulk plasma frequency, and γ_{bulk} is the bulk collision frequency. The second term, $\epsilon(\omega)_{\text{inter}}$, is due to interband transitions. The imaginary part of $\epsilon(\omega)_{\text{inter}}$ arises from interband transitions, and the real part is from the polarizability of the bound electrons (primarily the *d*-band electrons for gold).

A plasmon resonance is a cooperative electron effect, meaning that electron collisions result in a loss of electron phase coherence, which in turn results in a broadening of the plasmon absorption linewidth. Since the gold shells of these nanoparticles are thinner than the bulk electron mean free path in gold, a contribution to the dielectric function that is due to electron surface scattering becomes important. Several models, both quantum mechanical and classical, have been developed in an effort to describe experimentally observed plasmon resonance shifts and linewidths in solid metal nanoparticles that are due to electron surface scattering.[1] It is difficult to obtain precise information from experiments to compare with theory for two reasons. First, inhomogeneous broadening that is due to nanoparticle size and shape distributions makes it difficult to extract detailed information from linear optical studies. Second, an effect competing with (and related to) electron surface scattering is chemical interface damping, whereby the plasmon resonance and linewidth are modified by the local chemical environment.[3,34] Nonetheless, the simple phenomenological model we present explains the experimental linewidth narrowing that occurs during the gold nanoshell reaction.

When size-dependent electron scattering becomes important, the bulk collisional frequency can be modified as follows:

$$\Gamma = \gamma_{\text{bulk}} + Av_F/a, \quad (16)$$

where γ_{bulk} is the bulk collisional frequency described above, v_F is the Fermi velocity, and a is the reduced electron mean free path.[1] For gold nanoshells a is equated with the shell thickness, $(r_2 - r_1)$. A is a parameter determined by the geometry and theory used to derive this expression.[35] For simple Drude theory and isotropic scattering, $A = 1$.

Through this modification of the bulk collisional frequency, size-dependent electron scattering effects are easily incorporated into the Mie scattering calculations. We can modify the bulk dielectric function of the gold nanoshells as follows:

$$\epsilon(a, \omega) = \epsilon(\omega)_{\text{exp}} + \frac{{\omega_p}^2}{\omega^2 + i\omega\gamma_{\text{bulk}}} - \frac{{\omega_p}^2}{\omega^2 + i\omega\Gamma},$$

$$= \left(1 - \frac{{\omega_p}^2}{\omega^2 + i\omega\Gamma}\right) + \epsilon(\omega)_{\text{inter}}. \quad (17)$$

$\epsilon(a, \omega)$ is the size-dependent dielectric function, where $\epsilon(\omega)_{\text{exp}}$ is the experimental bulk dielectric function, and ω_p, γ_{bulk}, and Γ are as described previously.

The dashed curve in Fig. 5 shows a calculation of the extinction cross section with Eq. (17) used for the shell dielectric function. For comparison, the dashed–dotted curve shows the calculation that uses the unmodified bulk dielectric function. These calculations are for a 12.5-nm total radius particle with a shell thickness of 2.5 nm. The FWHM with electron surface scattering included is approximately 0.42 eV as compared with 0.075 eV when it is neglected.

Additionally, in any colloidal precipitation process there is a distribution of nanoparticle sizes. This leads to inhomogeneous broadening of the absorption spectrum. Therefore, to account for the population size distribution, r_2 is fitted with a Gaussian distribution. We assume a constant shell thickness $K = r_2 - r_1$ for the size distribution. For a given r_2, this determines r_1. The solid curve in Fig. 5 includes both surface electron scattering and a size distribution of ± 20 percent. The FWHM with this realistic population size distribution is 0.57 eV, which is 0.15 eV greater than the calculation that includes only surface electron scattering. Thus, for gold nanoshells in this size range, it is expected that homogeneous broadening that is due to electron surface scattering is the dominant contribution to the observed linewidth.

Figure 6 shows the results of calculations that use Mie theory in comparison with experiments. The solid curves are data, and the dotted curves are calculations that use Eq. (17) for the gold shell dielectric function. These calculations also include a population size distribution of ± 18 percent. The observed plasmon resonances correspond well to those calculated with Mie scattering theory at all times during the reaction. This analysis permitted us to relate the observed plasmon resonance shifts to the growth kinetics, thereby showing that the Au_2S core initially grows linearly in time, followed by linear time growth of the gold shell.[17] The observed linewidth narrowing that occurs during the course of the reaction can be understood with our model: As the shell grows

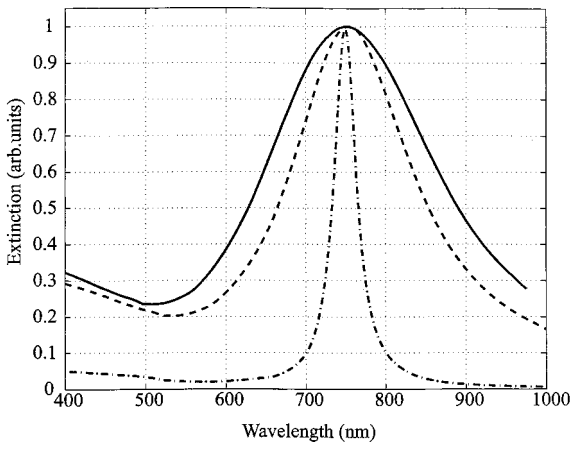

Fig. 5. Calculations of the plasmon resonance for a gold nanoshell with a core radius of 10 nm and a shell thickness of 2.5 nm. When electron surface scattering is taken into account, the FWHM increases from 0.075 to 0.42 eV (dotted–dashed curve and dashed curve, respectively). When a size distribution of ± 20 percent is included, the FWHM is 0.57 eV. Nonetheless, the dominant broadening mechanism is electron surface scattering.

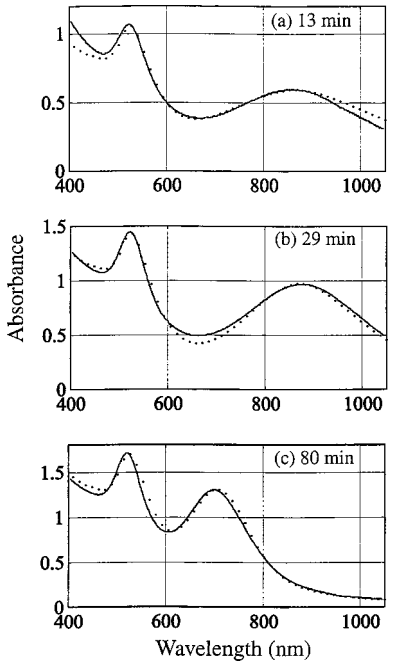

Fig. 6. UV-visible spectra of gold-coated Au_2S nanoshells at different times during the reaction. Solid curves, data; dotted curves, theory. The calculations yield (a) $r_1 = 8.6$ nm, $r_2 = 10.2$ nm; (b) $r_1 = 15.2$ nm, $r_2 = 17.9$ nm; (c) $r_1 = 15.2$ nm, $r_2 = 20.4$ nm. A modified version of Fig. 6 was presented in Ref. 17.

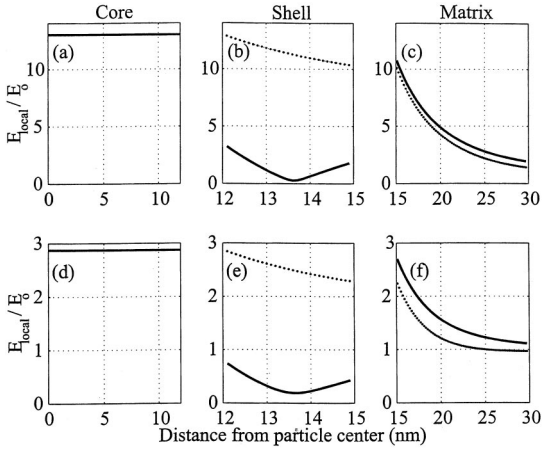

Fig. 7. Quasi-static calculations of the local electric field at the plasmon resonance versus radial distance. (a)–(c) Calculations for the field in the core, shell, and embedding medium, respectively, with the bulk dielectric function for gold. (d)–(f) The same calculations taking into account electron surface scattering. For these calculations, $r_1 = 12$ nm, $r_2 = 15$ nm, $\epsilon_1 = 5.44$, and $\epsilon_3 = 1.78$, giving a plasmon resonance at 750 nm. Solid curves, parallel to the incident field; dotted curves, perpendicular to the incident field.

thicker, the effect of surface electron scattering is reduced. In short, including both electron surface scattering and inhomogeneous broadening in our Mie calculations, the plasmon linewidth narrowing, in addition to the plasmon resonance shifts, can be accounted for as the nanoparticle growth reaction proceeds.

D. Local Fields

As a final point of interest regarding the electromagnetic response of gold nanoshells, the local electric field in and around the nanoparticles is considered. This is of interest because there can be a large field enhancement in the vicinity of solid nanoparticles. This large local field is important in surface-enhanced Raman scattering (SERS).[36,37] We recently demonstrated near-infrared SERS for molecules at the surface of metal nanoshells.[38] In addition, solid gold nanoparticles were shown to have a large third-order optical nonlinearity that was associated with the local-field enhancement.[7,39] For metal nanoshells the metal shell gives rise to field enhancement in the core, and it has been suggested that, for a semiconducting core, this could yield low-threshold optical bistability.[15,40]

Figure 7 shows calculations of the local field normalized to the incident field for a gold nanoshell with $r_1 = 12$ nm and $r_2 = 15$ nm. The calculations are in the quasi-static limit and use the equations for the fields shown above. Figures 7(a)–7(c) show the magnitude of the local field as a function of radial distance in the core, shell, and matrix, respectively, without including electron surface scattering. Each solid curve is the local field parallel to the incident field, and each dotted curve is the local field perpendicular to the incident field. The field in the core is homogeneous, and these calculations indicate an intensity enhancement of approximately 170 times the incident intensity. However, as mentioned previously, electron-surface-scattering effects must be included, since the shell thickness is less than the bulk electron mean free path for gold. Figures 7(d)–7(f) show the result of local-field calculations when electron surface scattering is taken into account by means of Eq. (17). The intensity in the core is enhanced only by a factor of 9 in this more realistic calculation. In general, for nanoparticles with dimensions smaller than the bulk electron mean free path, care must be taken when the magnitude of the local field is being determined. For example, a lower-field enhancement in the core results in a decrease in the magnitude of the third-order optical nonlinearity. The effect of electron surface scattering can be reduced for a particular wavelength by growing a larger core and a thicker shell (keeping the same ratio of r_1 to r_2), but then effects such as increased optical scattering must be considered. Recent work has examined the local fields of metal nanoshells both experimentally and theoretically in more detail.[41]

4. DISCUSSION

In the treatment of the plasmon resonance linewidths, only the dynamics of the Drude-like conduction electrons was modified to include size-dependent electron scattering. This was accomplished by separation of the bulk dielectric function of gold into a Drude free electron term and a term that is due to interband transitions (Eqs. 15 and 17). It is reasonable to expect a size dependence for the interband term as well, since with decreasing nanoparticle size, translational symmetry will eventually break down, as will the concept of band structure. In

fact, experimental studies on solid gold nanoparticles have demonstrated that the interband transition edge redshifts with decreasing nanoparticle size.[42] However, this deviation in the interband transition from bulk occurs only for gold nanoparticles with fewer than ~1000 atoms. During the course of the Au/Au_2S nanoparticle growth, the number of gold atoms in the shell ranges from $\sim 5 \times 10^3$ to $\sim 5 \times 10^5$. We therefore do not expect any size-dependent modifications of the interband term of the gold dielectric function, and our modification of only the Drude term in Eq. (17) is reasonable.

In bulk gold the 5*d*-band to conduction-band transition occurs near 2.4 eV. In pure gold colloid the plasmon resonance also occurs near 2.4 eV. Therefore in gold colloid the observed plasmon resonance is due to cooperative resonant oscillation of both the conduction electrons and *d*-band electrons that are optically excited into the conduction band. In contrast, the plasmon resonance in the gold nanoshell system is usually shifted to below 2.0 eV, which means that *d*-band electrons are not optically excited. For gold nanoshells this indicates that the plasmon resonance is due solely to the Drude-like conduction electrons. There is no increase in the conduction-electron population from *d*-band transitions. It is an interesting consequence of the shell geometry that only the conduction electrons of gold participate in the collective plasmon resonance. However, the electron dynamics in gold nanoshells shows that the *d*-band electrons do contribute to the photoinduced changes in transmission.[43]

In conclusion, we have investigated and analyzed the resonant optical properties of nanoparticles consisting of Au_2S cores and gold shells. These nanoshell nanoparticles have a tunable plasmon resonance that depends on the ratio of the core radius to the total radius. Additionally, the observed plasmon linewidth is dominated by electron surface scattering. In a subsequent paper the temporal dynamics of gold nanoshells are investigated with femtosecond pump–probe experiments.

ACKNOWLEDGMENTS

We thank D. Sarkar for his Mie scattering software, T. R. Lee for discussions regarding the functionalization of nanoshells, and S. J. Oldenburg for discussions regarding the local field. This work was supported by the Robert A. Welch Foundation, the Office of Naval Research, and National Science Foundation grant ECS-9801707.

S. Westcott and N. Halas can be reached at the address on the title page or by e-mail at westcott@rice.edu or halas@rice.edu.

*Present address: Materials Science and Technology Division, Los Alamos National Laboratory, New Mexico 87545; e-mail: raveritt@lanl.gov.

REFERENCES AND NOTES

1. U. Kreibig and M. Vollmer, *Optical Properties of Metal Clusters* (Springer, New York, 1995).
2. P. Mulvaney, "Surface plasmon spectroscopy of nanosized metal particles," Langmuir **12**, 788–800 (1996).
3. U. Kreibig, M. Gartz, and A. Hilger, "Mie resonances: sensors for physical and chemical cluster interface properties," Ber. Bunsenges. Phys. Chem. **101**, 1593–1604 (1997).
4. R. Elghanian, J. J. Storhoff, R. C. Mucic, R. L. Letsinger, and C. A. Mirkin, "Selective colorimetric detection of polynucleotides based on the distance-dependent optical properties of gold nanoparticles," Science **277**, 1078–1081 (1997).
5. S. Nie and S. R. Emory, "Probing single molecules and single nanoparticles by surface-enhanced Raman scattering," Science **275**, 1102–1106 (1997).
6. R. Antoine, P. F. Brevet, H. H. Girault, D. Bethell, and D. J. Schiffrin, "Surface plasmon enhanced non-linear optical response of gold nanoparticles at the air/toluene interface," J. Chem. Soc. Chem. Commun. 1901–1902 (1997).
7. D. Ricard, P. Roussignol, and C. Flytzanis, "Surface-mediated enhancement of optical phase conjugation in metal colloids," Opt. Lett. **10**, 511–513 (1985).
8. M. Brust, M. Walker, D. Bethell, D. J. Schiffrin, and R. Whyman, "Synthesis of thiol-derivatised gold nanoparticles in a two-phase liquid–liquid system," J. Chem. Soc. Chem. Commun. 801–802 (1994).
9. R. G. Freeman, K. C. Grabar, K. J. Allison, R. M. Bright, J. A. Davis, A. P. Guthrie, M. B. Hommer, M. A. Jackson, P. C. Smith, D. G. Walter, and M. J. Natan, "Self-assembled metal colloid monolayers: an approach to SERS substrates," Science **267**, 1629–1632 (1995).
10. R. P. Andres, J. D. Bielefeld, J. I. Henderson, D. B. Janes, V. R. Kolagunta, C. P. Kubiak, W. J. Mahoney, and R. G. Osifchin, "Self-assembly of a two-dimensional superlattice of molecularly linked metal clusters," Science **273**, 1690–1693 (1996).
11. C. P. Collier, R. J. Saykally, J. J. Shiang, S. E. Henrichs, and J. R. Heath, "Reversible tuning of silver quantum dot monolayers through the metal-insulator transition," Science **277**, 1978–1981 (1997).
12. H. R. Stuart and D. G. Hall, "Enhanced dipole–dipole interaction between elementary radiators near a surface," Phys. Rev. Lett. **80**, 5663–5666 (1998).
13. T. S. Ahmadi, Z. L. Wang, T. C. Green, A. Henglein, and M. A. El-Sayed, "Shape-controlled synthesis of colloidal platinum nanoparticles," Science **272**, 1924–1926 (1996).
14. A. L. Aden and M. Kerker, "Scattering of electromagnetic waves from two concentric spheres," J. Appl. Phys. **22**, 1242–1246 (1951).
15. A. E. Neeves and M. H. Birnboim, "Composite structures for the enhancement of nonlinear-optical susceptibility," J. Opt. Soc. Am. B **6**, 787–796 (1989).
16. H. S. Zhou, I. Honma, H. Komiyama, and J. W. Haus, "Controlled synthesis and quantum-size effect in gold-coated nanoparticles," Phys. Rev. B **50**, 12052–12056 (1994).
17. R. D. Averitt, D. Sarkar, and N. J. Halas, "Plasmon resonance shifts of Au-coated Au_2S nanoshells: insight into multicomponent nanoparticle growth," Phys. Rev. Lett. **78**, 4217–4220 (1997).
18. S. J. Oldenburg, R. D. Averitt, S. L. Westcott, and N. J. Halas, "Nanoengineering of optical resonances," Chem. Phys. Lett. **288**, 243–247 (1998).
19. A. J. Bard, R. Parsons, and J. Jordan, eds., *Standard Potentials in Aqueous Solution* (Marcel Dekker, New York, 1985).
20. G. Schmid and A. Lehnert, "The complexation of gold colloids," Angew. Chem. Int. Ed. Engl. **28**, 780–781 (1989).
21. The size distribution was determined with Image Tool for Windows, version 1.28, from the University of Texas Health Sciences Center at San Antonio.
22. G. Mie, "Beiträge zur optik trüber medien, speziell kolloidaler metallösungen," Ann. Phys. **25**, 377–445 (1908).
23. J. A. Stratton, *Electromagnetic Theory* (McGraw-Hill, New York, 1941).
24. M. Kerker, *The Scattering of Light and Other Electromagnetic Radiation* (Academic, New York, 1969).
25. C. F. Bohren and D. R. Huffman, *Absorption and Scattering of Light by Small Particles* (Wiley, New York, 1983).
26. D. Sarkar, "Vector basis function solution of Maxwell's equations," Ph.D. dissertation (Rice University, Houston, Texas, 1996).

27. D. Sarkar and N. J. Halas, "General vector basis function solution of Maxwell's equations," Phys. Rev. E **56**, 1102–1112 (1997).
28. J. W. Haus, H. S. Zhou, S. Takami, M. Hirasawa, I. Honma, and H. Komiyama, "Enhanced optical properties of metal-coated nanoparticles," J. Appl. Phys. **73**, 1043–1048 (1993).
29. H. C. van de Hulst, *Light Scattering by Small Particles* (Dover, New York, 1981).
30. Au_2S is a direct bandgap semiconductor with E_g in the range from 1.3 to 2.6 eV, O. Jepsen, Max-Planck-Institute for Solid State Research, D-7000 Stuttgart 80, Germany (personal communication, 1996).
31. J. I. Pankove, *Optical Processes in Semiconductors* (Dover, New York, 1975).
32. P. B. Johnson and R. W. Christy, "Optical constants of the noble metals," Phys. Rev. B **6**, 4370–4379 (1972).
33. N. W. Ashcroft and N. D. Mermin, *Solid State Physics* (Saunders, Philadelphia, 1976).
34. H. Hövel, S. Fritz, A. Hilger, U. Kreibig, and M. Vollmer, "Width of cluster plasmon resonances: bulk dielectric functions and chemical interface damping," Phys. Rev. B **48**, 18178–18188 (1993).
35. U. Kreibig and L. Genzel, "Optical absorption of small metallic particles," Surf. Sci. **156**, 678–700 (1985).
36. M. Moskovits, "Surface-enhanced spectroscopy," Rev. Mod. Phys. **57**, 783–826 (1985).
37. H. Metiu, "Surface enhanced spectroscopy," Prog. Surf. Sci. **17**, 153–320 (1984).
38. S. J. Oldenburg, S. L. Westcott, R. D. Averitt, and N. J. Halas, "Surface enhanced Raman scattering in the near infrared using metal nanoshell substrates," J. Chem. Phys. (to be published).
39. F. Hache, D. Ricard, C. Flytzanis, and U. Kreibig, "The optical Kerr effect in small metal particles and metal colloids: the case of gold," Appl. Phys. A **47**, 347–357 (1988).
40. J. W. Haus, N. Kalyaniwalla, R. Inguva, M. Bloemer, and C. M. Bowden, "Nonlinear-optical properties of conductive spheroidal particle composites," J. Opt. Soc. Am. B **6**, 797–807 (1989).
41. S. J. Oldenburg, G. D. Hale, J. B. Jackson, and N. J. Halas, "Light scattering from dipole and quadrupole nanoshell antennas," Appl. Phys. Lett. (to be published).
42. U. Kreibig, "The transition cluster–solid state in small gold particles," Solid State Commun. **28**, 767–769 (1978).
43. R. D. Averitt, S. L. Westcott, and N. J. Halas, "Ultrafast electron dynamics in gold nanoshells," Phys. Rev. B **58**, 10203–10206 (1998).